Proceedings World Geothermal Congress 2020+1
Reykjavik, Iceland, April - October 2021

Hot Dry Rocks and Their Geological Significance from Gonghe Basin at Northeast Margin of Qinghai-Tibet Plateau

Jianyun Feng, Ying Zhang and Jun Luo

Mailing address: SINOPEC Petroleum Exploration and Production Research Institute, Beijing 100083, China

E-mail address: fengjy.syky@sinopec.com

Keywords: Qinghai-Tibet Plateau, Gonghe Basin, Hot Dry Rock, Geochemistry, Geochronology

ABSTRACT

Gonghe Basin in the northeast margin of Qinghai-Tibet Plateau is a faulted basin formed in the Mesozoic era, controlled by large active dextral-slide faults, for instance, the Wahongshan fault in NNW direction to the west, and the Waligongshan and the Duohemao faults in NNW direction to the east. Based on regional geology, geothermal geology and integrated geophysical exploration results, the GR1 hot dry rock (HDR) exploration well was completed in the central part of Qiabuqia Town in Gonghe basin. The GR1 well is the highest temperature HDR exploration well in China, which has laid an important foundation for the first EGS demonstration project of China. The temperature measurement results show that the temperature at the depth of 2500m is 150°C, entering into the hot dry rock section. The temperature of the bottom hole at the depth of 3602.6m is 188.87°C. The average geothermal gradient of 2500-3705m is 71.4°C/km, which is higher than that of the other 3 hot dry rock exploration wells. At 2800-3705m depth in the GR1 well the geothermal gradient is higher than 80°C/km. The types of rocks related to the hot dry rocks are complicated and various, including volcanic and intrusive rocks. Volcanic rocks consist of basalt, andesite, dacite, rhyolite and volcanic breccia; intrusive rocks consist of gabbro, diorite, granodiorite, granite and quartz porphyry, etc. U-Pb isotopic chronology studies reveal that these igneous rocks are mostly crystallized in Anisian period of Middle Triassic (247-242 Ma). And the granitic plutons are considered to be derived from the same magma chamber and intruded into the upper crust contemporaneously. Geochemistry characteristics and rock assemblages suggest that the Middle Triassic igneous rocks are formed in a continental margin arc setting by the northern subduction of Paleo-Tethys ocean. The early preexisting horizontal fractures in GR1 indicate that the granite is naturally fractured and are propitious to form a connected fracture network within 3200 m-3705 m depth. This network is conducive to the formation of complex heat exchange paths according to reservoir stimulation. Consequently, the Qiabuqia site is believed suitable for establishing an EGS power generation system in China.

1. INTRODUCTION

Renewable and green energy has been used more and more extensively in solving the issues between booming economy and environmental degradation since 2000. Therefore, as a clean, environment-friendly and constant energy source, geothermal energy has been exploited and utilized to generate electricity, heat space or facilitate industry (Ahmadi et al., 2013; Habka and Ajib, 2013; Tester et al., 2006; Zarrouk and Moon, 2014). The hot dry rock (HDR) energy is the most abundant and high-quality type in geothermal, and is stored in hot and low permeable crystalline and other rocks within 3-10 km depths, and the total amount of HDR energy resource in mainland China reaches 25×10^6EJ (Wang et al., 2013). Nevertheless, as HDR is deeply buried and commonly with low permeability for heat extraction, the effective exploitation of HDR heat is challenging, requiring the permeability enhancement by enhanced or engineered geothermal system (EGS) (Tester et al., 2006). Over ten EGS projects have been built and tested in the world in the past 50 years, including Fenton Hill, Raft River, Desert peak and Geysers projects in the United States, Rosemanows project in UK, Soultz project in France, Ogachi and Hijiori projects in Japan, Landau project in Germany, Cooper Basin project in Australia (Tester et al., 2006; Xie and Min, 2016; Ziagos et al., 2013). These projects try to extract heat from HDR by drilling deep wells to create a connected fracture network in the reservoir. There is still no successfully commercialized EGS plant except Soultz for economic and technologic reasons. China began to study HDR in the last two decades with a minor whole-country HDR resource survey and a few HDR boreholes in the Zhangzhou and Gonghe areas. In the exploration holes of GR1 carried out in one of the hot dry rock masses of the Qiabuqia HDR in the Gonghe area, the temperature at the depth of 3602.6m at the hole bottom reached 188.97°C. Based on isotopic and geochemical analysis on the Qiabuqia HDR, the paper tries to illustrate geochronology and petrogenesis of the HDR, and give shed some light on the geological setting and forming mechanism of the HDR in the area.

2. GEOLOGICAL SETTING

The Gonghe Basin is located in the northeast of the Qinghai-Tibet Plateau and lies between the Qilian, Kunlun and the Qinling Mountains, and is called “Qin-Kun Fork” and “Gonghe Gap”. As a Cenozoic rhombic intermontane basin, the Gonghe-Guide area is surrounded by the Qinghai South Mountain to the north, Heka South Mountain to the south, Ela Mountain to the west and Zhama Mountain to the east and is divided into the Gonghe and Guide basins by the Waligong tectono-magmatic belt (Sun et al., 2011; Wang et al., 2015). This basin is 210 km long from east to west with 50 km width from south to north, and has a total area of about 12,000 km2. The major tectonic structures in the Gonghe-Guide area are NW-NWW and NNW strike-slip faults (Fig. 1). The NW-NWW faults include the Qinghai South Mountain fault and Heka South Mountain fault. While the NNW strike-slip faults in the study area are represented by the Ela Mountain and Waligong fault zones. The Zhacang Temple and Qunaihai hot springs, as well as Xinjie hot spring scattered along the Waligong fault, indicates that the fault might serve as a transport channel for the upward convection of deep geothermal fluids, through which the latest hydrothermal activities occurred in the Quaternary (Bao et al., 2009). The highest spring temperature is 93.5°C. The NW-NWW sinistral strike-slip faults in the area were formed in the nearly S-N and N-E tectonic compressive stress field associated with the ongoing collision between the India and Eurasian plates since the late Mesozoic (Tapponnier et al., 2001; Yin and Harrison, 2003). The NNW deep faults are well developed on the northern Qinghai-Tibet Plateau and were formed by compression and thrusting from west to east (Hou et al., 1999).

The basement rock in the Gonghe Basin is composed of Middle Triassic igneous rocks, which is considered to be the deep HDR reservoir. Zhang et al. (2006) reported that the main igneous rocks in the area were granite and granodiorite. Two stages of plutonic intrusions were identified by the analysis of a U-Pb zircon LA-ICP MS geochronology: the early Carnian stage of Late Triassic (the first stage), which was represented by the Hemahe intrusion with a U-Pb zircon age of 235 Ma, and the middle Norian stage of Late Triassic, 218 Ma for the Wenquan intrusion (the second stage). Based on the geochemical properties of the granodiorite samples, they suggested that the original magma was generated from the partial melting of the lower crust beneath the area. The basement is overlain by thick Paleogene, Neogene and Quaternary lacustrine strata (Xue et al., 2013). Two shallow thermal reservoirs have been identified in sedimentary cap layers: a lower Pliocene reservoir of fine and coarse grain sandstone, and a Miocene reservoir of sandstone and gravel-bearing sandstone (Yan et al., 2013). The Gonghe area was studied in the past few years for terrestrial heat flow, crustal thermal structure, geothermal formation mechanism, EGS, Cenozoic tectonic evolution, and HDR improving the breadth and depth of understanding about the HDR potential in the area (Feng et al., 2018; Lei et al., 2019; Lu et al., 2012; Xie et al., 2015; Xu et al., 2018; Zhang et al., 2018a, b).

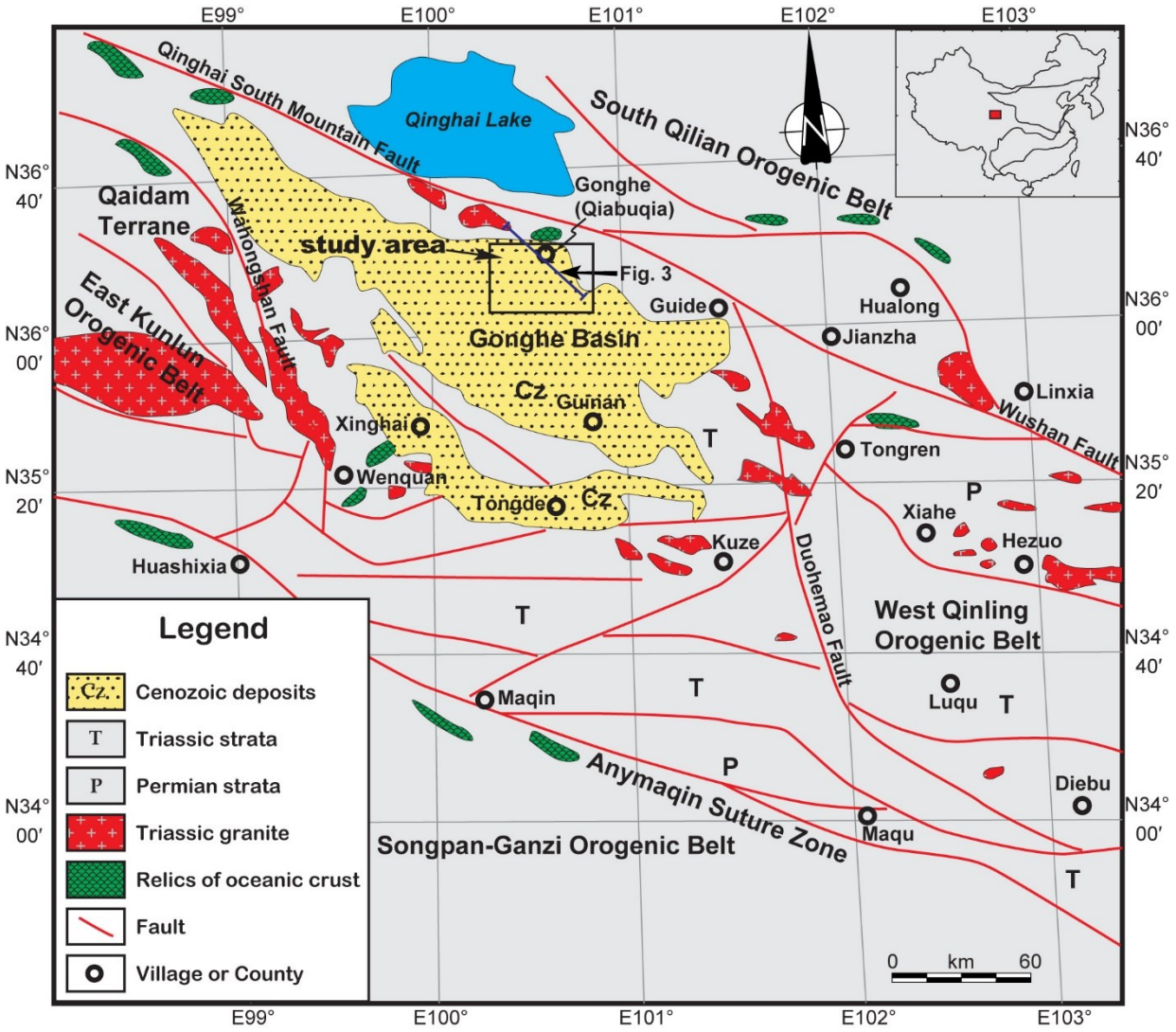

Fig.1. Simplified geological map of Gonghe Basin and its adjacent areas (modified after Xie et al., 2015)

3. METHODOLOGY

Eleven granite samples, numbered from 18GH-01 to 18GH-11, were collected from drilling cores of GR1 and GR2 in Qiabuqia Village of the Gonghe basin. The samples of 18GH-01, 18GH-02, 18GH-05, 18GH-06 and 18GH-07 were selected intermittently from 2450m to 3000m depth from GR1 core, and the other 6 ones were from 2130m to 3000m from GR2.

3.1 In-situ U-Pb dating and trace element analysis of zircon by LA-ICP-MS

U-Pb dating and trace element analysis of zircon were simultaneously conducted by LA-ICP-MS at the Wuhan Sample Solution Analytical Technology Co., Ltd., Wuhan, China. Detailed operating conditions for the laser ablation system and the ICP-MS instrument and data reduction are the same as in the description by Zong et al. (2017). Laser sampling was performed using a GeolasPro laser ablation system that consists of a COMPexPro 102 ArF excimer laser (wavelength of 193nm and maximum energy of 200mJ) and a MicroLas optical system. An Agilent 7700e ICP-MS instrument was used to acquire ion-signal intensities. Helium was applied as a carrier gas. Argon was used as the make-up gas and mixed with the carrier gas via a T-connector before entering the ICP. A “wire” signal smoothing device is included in this laser ablation system (Hu et al., 2015). The spot size and frequency of the

laser were set to 32μm and 5Hz, respectively, in this study. Zircon 91500 and glass NIST610 were used as external standards for U-Pb dating and trace element calibration, respectively. Each analysis incorporated a background acquisition of approximately 20-30s followed by 50s of data acquisition from the sample. An Excel-based software ICPMSDataCal was used to perform off-line selection and integration of background and analyzed signals, time-drift correction and quantitative calibration for trace element analysis and U-Pb dating (Liu et al., 2008, 2010). Concordia diagrams and weighted mean calculations were made using Isoplot/Ex_ver3 (Ludwig, 2003).

3.2 Major element analyses of whole rock

Major element analyses of whole rock were conducted on XRF (Primus II, Rigaku, Japan) at the Wuhan Sample Solution Analytical Technology Co.,Ltd., Wuhan, China. The detailed sample-digesting procedure was as follows: (1)Sample powder (200 mesh) were placed in an oven at 105°C for drying of 12 hours; (2) ~1.0g dried sample was accurately weighted and placed in the ceramic crucible and then heated in a muffle furnace at 1000°C for 2 hours. After cooling to 400°C, this sample was placed in the drying vessel and weighted again in order to calculate the loss on ignition(LOI); (3) 0.6g sample powder was mixed with 6.0g cosolvent ($Li_2B_4O_7$: $LiBO_2$: LiF = 9:2:1) and 0.3g oxidant (NH_4NO_3) in a Pt crucible, which was placed in the furnace at 1150°C for 14 mins. Then, this melting sample was quenched with air for 1 min to produce flat discs on the fire brick for the XRF analyses.

3.3 Trace element analyses of whole rock

Trace element analysis of whole rock were conducted on an Agilent 7700e ICP-MS at the Wuhan Sample Solution Analytical Technology Co., Ltd., Wuhan, China. The detailed sample-digesting procedure was as follows: (1) Sample powder (200 mesh) were placed in an oven at 105°C for drying of 12 hours; (2) 50mg sample powder was accurately weighed and placed in a Teflon bomb; (3) 1ml HNO_3 and 1ml HF were slowly added into the Teflon bomb; (4) Teflon bomb was put in a stainless steel pressure jacket and heated to 190°C in an oven for >24 hours; (5) After cooling, the Teflon bomb was opened and placed on a hotplate at 140°C and evaporated to incipient dryness, and then 1ml HNO_3 was added and evaporated to dryness again; (6) 1ml of HNO_3, 1ml of MQ water and 1 ml internal standard solution of 1ppm In were added, and the Teflon bomb was resealed and placed in the oven at 190°C for >12 hours; (7) The final solution was transferred to a polyethylene bottle and diluted to 100g by the addition of 2% HNO_3.

4. ANALYSIS RESULT AND DISCUSSION OF HDR RESERVOIR

4.1 Petrology

The drilling cores revealed that the geothermal convective system in Gonghe Basin consists of shallow and deep reservoirs. The shallow reservoir in depths of 100-200m is composed of Cenozoic loose or semi-consolidated porous deposits. The deep reservoir is buried between -669m and -1150m underground, widely underlain by granite hot dry rocks and is dominated by natural cracks or fissures. The deep reservoir mainly consists of intermediate and acidic plutons, including reddish porphyritic monzogranite, grey biotite granite, grey granodiorite, altered biotite granite and biotite monzogranite, etc. All these granitoids are middle or coarse grain and massive structure (Fig.2).

Fig.2. Outcrops and borehole cores of the Qiabuqia granite. a. Outcrop of the massive granite with parallel joints at Longcaigou site of Qiabuqia Village; b. Concentrate parallel joints across the K-feldspar crystal at Longcaigou site of Qiabuqia Village; c. Natural horizontal fractures and high-angle fracture filled with Calcite vein from borehole core of GR1; d. Rock-core disking in GR2 at the depth of 3380m.

All the samples are grey middle to coarse grain granodiorite and biotite granite, and are fresh and clean for geochemical analyzing without fluid alteration and metamorphism. And the samples are composed mainly of quartz, K-feldspar, plagioclase, biotite, amphibole and apatite, etc. Diameters of most minerals are bigger than 2mm, with 20mm as a maximum. The petrological features implies a deep-seated origin and slow crystallization for their perfect crystalline form and big-size phenocrysts. Thus high-quality heat flow will be saved in the plutons for a long time in geochronology.

4.2 Temperature of the HDR reservoir

In the Qabqa area, ten geothermal exploration wells were drilled, four of which have a bottom-hole temperature of more than 178°C, i.e. DR3, DR4, GR1 and GR2 (Fig. 1c). The rock temperature reaches 180.27°C at 2927.2m depth underground in well DR3. According to the DR4 drilling data, the depth of the granite roof is 1400 m, when the hole depth is 3086 m, the rock temperature reaches 179°C; when the hole depth is 3102 m, the rock temperature is 178.72°C. The bottom-hole temperature of GR2 also reaches 180°C at the depth of 3000m in granite. Most importantly, the bottom-hole temperature of GR1 well that terminated at 3705 m depth in March 2017, was continuously monitored by high precision stationary point thermometers to reach approximately 236°C, which is considered to be the most successful geothermal drilling in the Qiabuqia site (Fig.3) . The temperature of the bottom hole was remeasured recently at the depth of 3602.6m in GR1 and is 188.87°C. Drilling boreholes show that the geothermal gradient varies with depth as follows: 1-4°C/100 m in Quaternary strata (Q), 4.6-5.3°C/100 m in Neogene strata (N), and about 7.1°C/100 m in granite. Most importantly, all the wells encountered no water when drilled into the granitic rocks, indicating an ideal target for Hot Dry Rock development.

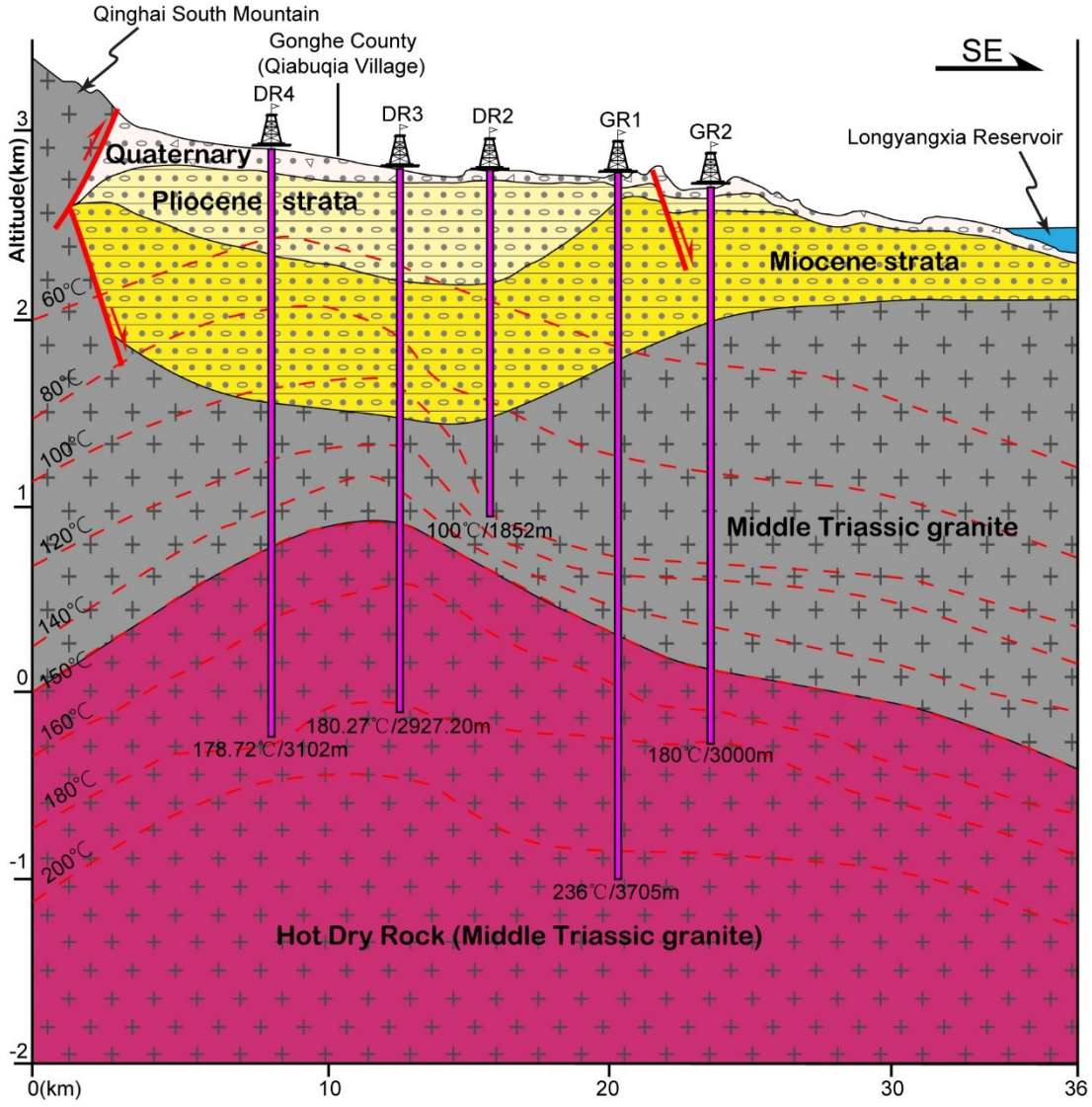

Fig.3. Qiabuqia geothermal field model interpreted by drilling. Location of the section was marked in Fig.1.

On the drilling cores from the GR1 borehole from 3200 m to 3705 m depth, as shown in Fig. 2d, the natural or preexisting fracture density of cores in the horizontal direction increases downwards significantly. These fractures are featured differently than the late natural fractures formed by rock-core disking and the early preexisting fractures filled with major calcites and minor quartzes. Drilling core disking is common in borehole triggered by the sudden release of high crustal stress, implying a high-stress geological environment. The early preexisting fractures indicate that the granite are naturally fractured and are propitious to form a connected fracture network within 3200 m-3705 m depth, which are conducive to the formation of complex heat exchange paths during reservoir stimulation (Ziagos et al., 2013).

Compared with the Soultz site in France, which has a high reservoir temperature of 200°C at 5000 m depth (Genter et al., 2010), the Qiabuqia site is more favorable for an EGS project, having a lower reservoir temperature of 188.87°C, shallower burial of less than 4000m, a stable heat supply, and a naturally fractured reservoir. Consequently, the Qiabuqia site is believed suitable for establishing an EGS power generation system in China.

4.3 Geochronology

For the sample 18GH-01 of borehole GR1, fifteen U–Pb analyses of the oscillatory-zoned cores yielded high concentrations of U (1344–6972 ppm) and Th (601–2343 ppm), with Th/U ranging 0.26–0.64，indicating a typical magma origin (Table 1). The $^{206}Pb/^{238}U$ versus $^{207}Pb/^{235}U$ diagram indicates that fifteen oscillatory-zoned cores have $^{206}Pb/^{238}U$ ages between 249.6 ± 1.7 Ma and 249.6 ± 2.2 Ma, with a mean $^{206}Pb/^{238}U$ age of 243.7 ± 1.8Ma (MSWD =2.7; Fig. 4a).

For the sample 18GH-04 of borehole GR2, twenty-eight U–Pb analyses of the oscillatory-zoned cores yielded high concentrations of U (2305–6356 ppm) and Th (603–2228 ppm), with Th/U ranging 0.20–0.75, similar as 18GH-01 of a magma origin (Table 2). The $^{206}Pb/^{238}U$ versus $^{207}Pb/^{235}U$ diagram indicates that twenty-eight oscillatory-zoned cores have $^{206}Pb/^{238}U$ ages between 234.0 ± 1.8 Ma and 259.3 ± 2.5 Ma, with a mean $^{206}Pb/^{238}U$ age of 245.3 ± 2.7Ma (Table 2) (MSWD =11.2; Fig. 4b).

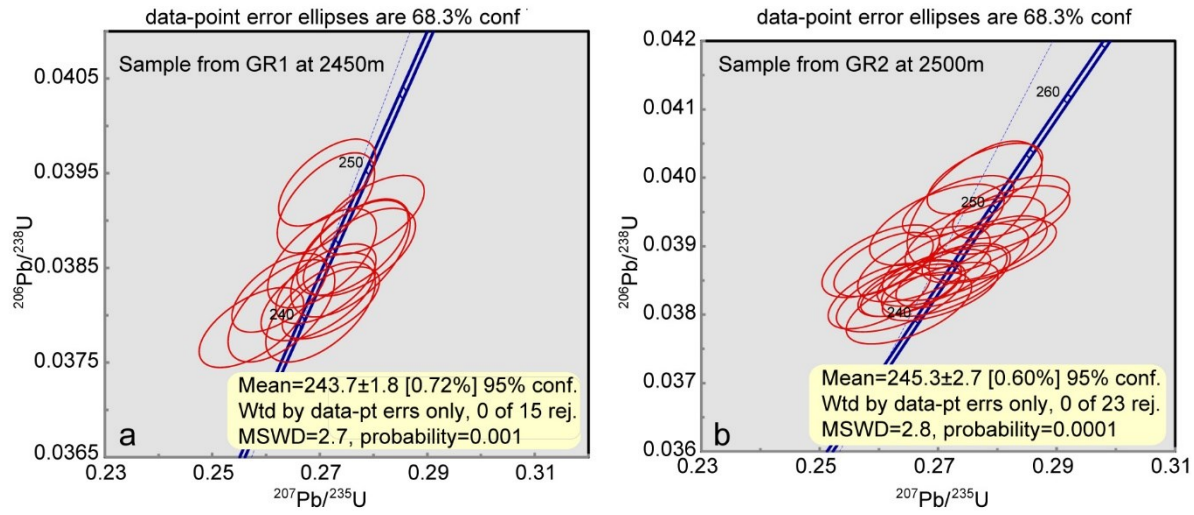

Fig.4. U–Pb concordia diagrams for the Qiabuqia granite from borehole cores of GR1 (a) and GR2 (b)

U-Pb isotopic chronology studies reveal that the forming ages of these igneous rocks are mostly crystallized in Anisian period of Middle Triassic (247-242 Ma). And the granitic plutons are considered to be derived from the same magma chamber and intruded into the upper crust contemporaneously. Even though the rocks were formed in the Triassic, the geothermal stored therein may not originate from the intruded time, and most probably is derived from Cenozoic tectonic events that cause the heat flow from a deep seated magma chamber or asthenosphere along Crust faults.

4.4 Whole-rock major and trace elements

The granite represented by cores of GR1 and GR2 display a concentrated and narrow variation in major and trace element composition (Table 3). They are characterized by low TiO_2 (0.22–0.49 wt%), $^{T}Fe_2O_3$ (1.96–4.20 wt%), P_2O_5 (0.03–0.13 wt%), MgO (0.54–1.44 wt%), CaO (1.62–3.76 wt%) contents and relatively high Na_2O (2.88–6.20 wt%) and K_2O (2.51–5.36 wt%) contents (Table 3). The primitive-mantle-normalized spidergram indicates that the granites are significantly enriched with some large-ion lithophile elements (LILEs, e.g., Rb, and Pb) and depleted with high field strength elements (HFSEs, e.g., Nb, Ta, Zr, Ce and HREE) with pronounced negative Sr and Ba anomalies (Fig. 5a). They show LREE-enriched chondrite-normalized REE patterns with negative Eu anomalies (0.35–0.70), similar to present-day OIB (Fig. 5b). All of the samples are featured by similar distribution patterns and tendencies in chondrite-normalized REE patterns and primitive mantle-normalized trace element diagrams, indicating a homogenous magma origin of oceanic island that is enriched in LILEs, Na_2O and K_2O but has negative anomalies in HFSEs.

Geochemistry characteristics and rock assemblages suggest that the Middle Triassic igneous rocks are formed in a continental margin arc setting by the northern subduction of Paleo-Tethys Ocean. All these also indicate that the geothermal energy in the rocks may not be formed from the crystallized time.

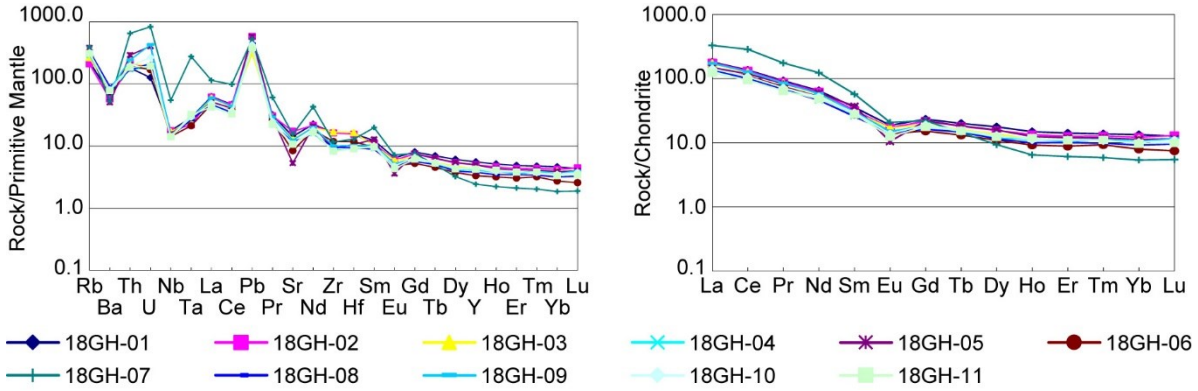

Fig.5. Diagrams of primitive mantle-normalized trace element (a) and chondrite-normalized REE patterns (b) for granite borehole cores from GR1 and GR2 in Qiabuqia Village of Gonghe Basin. Chondrite-normalized values are from Boynton (1984). Primitive mantle-normalized values are from Sun and McDonough (1989).

5. CONCLUSION

Gonghe Basin in northeast margin of Qinghai-Tibet Plateau is a faulted basin formed since the Mesozoic era. It is believed that granitic HDR developed widely in Qiabuqia Village of Gonghe Basin revealed by geothermal boreholes, particularly for the GR1 well that has a bottom-hole temperature of 188.87°C at the depth of 3602.6m. The conclusions obtained are as follows:

(1) The deep HDR reservoir mainly consists of intermediate and acidic plutons, i.e. granite. U-Pb isotopic chronology studies reveal that these igneous rocks are mostly crystallized in the Anisian period of Middle Triassic (247-242 Ma), which are considered to be derived from the same magma chamber and intruded into the upper crust contemporaneously. Even though the rocks were formed in the Triassic, the geothermal stored therein may not originate from the intruded time, and are probably derived from Cenozoic tectonic events that cause the heat flow from a deep-seated magma chamber or asthenosphere along Crust faults.

(2) Geochemistry characteristics and rock assemblages suggest that the Middle Triassic igneous rocks are formed in a continental margin arc setting by the northern subduction of Paleo-Tethys Ocean. The petrological features implies a deep-seated origin and slow crystallization for their perfect crystalline form and big-size phenocrysts. Thus high-quality heat flow will be saved in the plutons for a long time in geochronology.

(3) The early preexisting horizontal fractures in GR1 indicate that the granite are naturally fractured and are propitious to form a connected fracture network within 3200 m-3705 m depth, which are conducive to the formation of complex heat exchange paths during reservoir stimulation. Consequently, the Qiabuqia site is believed to be suitable for establishing an EGS power generation system in China although a tentative on-site test is planned in the area without energy production.

ACKNOWLEDGMENTS

This study was supported by the Consulting Research Project of Chinese Academy of Engineering (No.2019-XZ-35).

Table 1 LA–ICP–MS zircon U–Pb data for granite borehole core from GR1 in Qiabuqia Village of Gonghe Basin

Analyzed points	Content(10^{-6})			Th/U	Ratios						Age (Ma)					
	Pb	Th	U		$^{207}Pb/^{206}Pb$	1σ	$^{207}Pb/^{235}U$	1σ	$^{206}Pb/^{238}U$	1σ	$^{207}Pb/^{206}Pb$	1σ	$^{207}Pb/^{235}U$	1σ	$^{206}Pb/^{238}U$	1σ
18GH-01 granite sample from GR1, oscillatory-zoned cores																
18GH-01-17	234.9163	1058.5693	2216.9412	0.4775	0.0491	0.0013	0.2573	0.0064	0.0379	0.0003	150.1	54.6200	232.5	5.1927	239.6	1.7340
18GH-01-25	364.9343	1671.9906	2425.5768	0.6893	0.0514	0.0013	0.2701	0.0067	0.0380	0.0003	257.5	59.2475	242.8	5.3866	240.6	2.1684
18GH-01-13	334.6906	1475.0750	2977.7385	0.4954	0.0498	0.0012	0.2629	0.0066	0.0380	0.0004	187.1	55.5450	237.0	5.2758	240.7	2.2164
18GH-01-15	295.0278	1137.9986	3365.4816	0.3381	0.0515	0.0012	0.2720	0.0060	0.0381	0.0003	264.9	56.4750	244.3	4.7712	241.2	1.5614
18GH-01-19	349.6695	1533.8071	2842.7490	0.5396	0.0508	0.0013	0.2697	0.0070	0.0382	0.0003	235.3	63.8775	242.5	5.6205	241.6	1.9051
18GH-01-04	242.2311	859.3883	3252.9902	0.2642	0.0496	0.0011	0.2625	0.0058	0.0382	0.0003	176.0	51.8425	236.7	4.6901	241.9	1.7107
18GH-01-10	318.3183	1323.4702	3047.2098	0.4343	0.0511	0.0012	0.2712	0.0062	0.0383	0.0003	255.6	53.6950	243.6	4.9153	242.5	1.7265
18GH-01-24	321.8563	1297.2623	3070.7635	0.4225	0.0505	0.0012	0.2704	0.0067	0.0386	0.0003	216.7	54.6200	243.0	5.3379	244.2	2.1533
18GH-01-03	163.7857	680.4885	1404.2231	0.4846	0.0520	0.0014	0.2757	0.0073	0.0386	0.0004	283.4	62.9550	247.2	5.8370	244.2	2.5573
18GH-01-16	221.6512	868.0483	2481.6110	0.3498	0.0518	0.0013	0.2774	0.0069	0.0387	0.0003	276.0	57.4000	248.6	5.4794	244.6	1.9031
18GH-01-26	418.7343	1851.8416	3047.5543	0.6076	0.0515	0.0013	0.2761	0.0068	0.0387	0.0003	264.9	57.4000	247.6	5.4369	244.9	2.0592
18GH-01-11	275.6660	944.2543	3574.3844	0.2642	0.0517	0.0012	0.2798	0.0064	0.0391	0.0003	272.3	51.8450	250.5	5.0572	247.0	1.7117
18GH-01-09	339.2649	1455.0060	3076.8738	0.4729	0.0501	0.0011	0.2711	0.0060	0.0392	0.0003	198.2	51.8425	243.6	4.7797	247.8	2.1718
18GH-01-18	330.4180	1140.9048	4426.8406	0.2577	0.0496	0.0011	0.2714	0.0060	0.0394	0.0003	189.0	51.8425	243.8	4.7563	249.1	1.8849
18GH-01-01	154.7734	635.9210	1344.1417	0.4731	0.0522	0.0016	0.2861	0.0095	0.0395	0.0004	294.5	72.2150	255.5	7.4680	249.6	2.2338

Table 2 LA–ICP–MS zircon U–Pb data for granite borehole cores from GR2 in Qiabuqia Village of Gonghe Basin

Analyzed points	Content(10^{-6})			Th/U	Ratios						Age (Ma)					
	Pb	Th	U		$^{207}Pb/^{206}Pb$	1σ	$^{207}Pb/^{235}U$	1σ	$^{206}Pb/^{238}U$	1σ	$^{207}Pb/^{206}Pb$	1σ	$^{207}Pb/^{235}U$	1σ	$^{206}Pb/^{238}U$	1σ
18GH-04 granite sample from GR2, oscillatory-zoned cores																
18GH-04-07	144.5367	554.7219	1723.4460	0.3219	0.0522	0.0016	0.2716	0.0079	0.0377	0.0004	294.5	72.2150	244.0	6.3391	238.5	2.2133
18GH-04-30	151.1606	502.5218	2185.2093	0.2300	0.0502	0.0013	0.2651	0.0070	0.0381	0.0003	205.6	61.1000	238.7	5.6184	241.0	2.1539
18GH-04-13	209.4172	773.6161	2704.8413	0.2860	0.0497	0.0013	0.2637	0.0072	0.0383	0.0003	189.0	61.1000	237.8	5.7823	242.1	2.1381
18GH-04-27	275.8604	983.8144	3607.7470	0.2727	0.0490	0.0011	0.2601	0.0057	0.0383	0.0003	150.1	49.9950	234.7	4.6056	242.1	1.9640
18GH-04-20	258.6159	1067.6780	2873.8368	0.3715	0.0510	0.0012	0.2704	0.0065	0.0383	0.0003	239. 0	55.5450	243.0	5.1654	242.5	1.7531
18GH-04-22	303.3872	1133.8372	3946.1498	0.2873	0.0500	0.0011	0.2654	0.0056	0.0384	0.0003	198.2	54.6200	239.0	4.4739	242.6	1.5710
18GH-04-14	313.2113	1108.8230	4148.6514	0.2673	0.0499	0.0011	0.2652	0.0058	0.0384	0.0003	187.1	19.4400	238.9	4.6261	242.8	1.7035
18GH-04-11	270.4407	1106.4413	2536.8006	0.4362	0.0509	0.0014	0.2713	0.0072	0.0385	0.0004	235.3	62.9525	243.7	5.7441	243.6	2.1869
18GH-04-19	289.4889	1057.9012	3947.3985	0.2680	0.0504	0.0012	0.2693	0.0063	0.0385	0.0003	216.7	83.3200	242.1	5.0687	243.8	1.7070
18GH-04-23	280.9705	964.3556	3643.4042	0.2647	0.0510	0.0012	0.2723	0.0062	0.0386	0.0003	242.7	53.6925	244.5	4.9413	243.9	1.8603
18GH-04-15	259.1960	868.0648	3679.5683	0.2359	0.0486	0.0010	0.2608	0.0055	0.0387	0.0003	127.9	48.1450	235.3	4.4562	245.0	1.9214
18GH-04-04	215.3746	891.2858	2148.2038	0.4149	0.0497	0.0013	0.2676	0.0074	0.0387	0.0004	189. 0	62.9525	240.8	5.9127	245.0	2.2764
18GH-04-25	224.0556	895.8129	2309.4733	0.3879	0.0509	0.0015	0.2729	0.0081	0.0388	0.0004	235.3	68.5050	245.0	6.4890	245.2	2.3039
18GH-04-10	199.9346	745.3250	2297.0393	0.3245	0.0485	0.0012	0.2603	0.0065	0.0388	0.0003	124.2	61.1050	234.9	5.2763	245.3	2.1753
18GH-04-18	194.0067	767.6946	2144.3874	0.3580	0.0518	0.0014	0.2786	0.0075	0.0389	0.0003	276. 0	62.9550	249.6	5.9431	246.2	1.9184
18GH-04-21	263.5356	1119.7318	2469.3450	0.4535	0.0517	0.0012	0.2784	0.0066	0.0390	0.0003	272.3	53.6950	249.4	5.2340	246.4	1.9635
18GH-04-06	193.4049	691.1232	2370.0198	0.2916	0.0508	0.0014	0.2763	0.0078	0.0392	0.0004	231.6	66.6550	247.7	6.2234	247.6	2.3648
18GH-04-12	196.9642	696.5956	2392.3818	0.2912	0.0497	0.0014	0.2698	0.0075	0.0393	0.0004	189.0	66.6550	242.5	5.9939	248.6	2.4354
18GH-04-17	252.2397	1051.2854	2553.7628	0.4117	0.0517	0.0014	0.2812	0.0073	0.0394	0.0003	333.4	59.2525	251.6	5.7700	249.0	2.0529
18GH-04-08	221.5641	581.3165	3864.4214	0.1504	0.0514	0.0012	0.2823	0.0065	0.0396	0.0003	257.5	49.0675	252.5	5.1569	250.2	1.8955
18GH-04-16	261.1404	869.2340	3746.1575	0.2320	0.0499	0.0011	0.2734	0.0062	0.0396	0.0003	190.8	21.2925	245.4	4.9493	250.3	1.8320
18GH-04-29	310.2957	1064.6810	4441.6656	0.2397	0.0501	0.0011	0.2762	0.0075	0.0396	0.0006	198.2	51.8425	247.6	5.9820	250.4	3.8097
18GH-04-03	254.3494	801.5585	3456.5659	0.2319	0.0501	0.0012	0.2779	0.006	0.0400	0.0003	198.2	53.6950	249.0	5.1117	252.8	2.1228

Table 3 Whole-rock element concentrations for granite borehole cores from GR1 and GR2 in Qiabuqia Village of Gonghe Basin

	18GH-01	18GH-02	18GH-03	18GH-04	18GH-05	18GH-06	18GH-07	18GH-08	18GH-09	18GH-10	18GH-11
SiO_2	67.97	66.36	69.52	68.28	69.64	69.11	61.97	67.46	67.67	68.03	67.42
TiO_2	0.48	0.49	0.43	0.35	0.22	0.33	0.35	0.37	0.38	0.35	0.38
Al_2O_3	15.15	16.10	14.63	14.85	14.39	14.83	20.19	14.98	15.05	14.77	14.95
$^{T}Fe_2O_3$	4.03	3.99	3.62	3.48	1.96	2.82	2.60	3.65	3.82	3.96	4.20
MnO	0.07	0.10	0.07	0.06	0.04	0.05	0.06	0.07	0.07	0.07	0.07
MgO	1.33	1.44	1.12	0.99	0.54	1.05	0.60	1.06	1.09	1.11	1.22
CaO	3.76	2.87	3.05	2.76	2.86	1.62	3.19	3.15	2.96	2.95	3.22
Na_2O	3.25	3.93	2.92	3.56	3.11	3.64	6.20	2.88	3.43	3.21	3.15
K_2O	3.03	2.51	3.89	3.86	5.36	4.26	3.08	3.95	3.82	3.74	3.67
P_2O_5	0.13	0.13	0.11	0.08	0.09	0.07	0.03	0.09	0.09	0.08	0.08
LOI	0.65	1.78	0.67	1.53	1.66	2.17	1.42	2.05	1.63	1.28	1.19
SUM	99.84	99.70	100.02	99.80	99.88	99.94	99.68	99.70	100.02	99.54	99.54
Li	82.76	202.57	64.38	81.41	65.71	99.65	95.03	100.93	87.28	102.48	98.00
Be	3.10	3.95	2.36	4.00	2.98	2.82	27.68	3.37	3.66	3.94	3.43
Sc	8.37	7.95	7.55	6.05	5.39	6.24	3.67	6.05	6.09	6.95	7.35
V	37.26	37.15	30.78	27.49	15.72	24.86	11.91	30.27	29.59	29.66	33.41
Cr	12.60	13.25	9.86	24.07	5.22	9.31	5.82	39.87	26.34	39.53	44.75
Co	7.88	7.16	6.33	6.27	3.15	5.62	7.58	7.57	6.41	8.16	7.27
Ni	5.57	6.17	4.71	8.81	2.60	3.97	4.91	8.07	8.37	9.67	8.84
Cu	2.00	3.81	1.32	7.25	9.25	1.42	58.56	4.93	5.49	7.82	5.84
Zn	51.93	90.34	46.33	46.78	32.13	38.84	33.24	47.07	45.67	59.71	44.75
Ga	18.94	19.62	17.66	17.56	13.81	16.12	32.89	18.59	18.23	18.50	18.52
Rb	147.13	133.28	169.20	185.21	242.82	205.85	249.26	216.23	185.61	202.69	196.06
Sr	300.97	362.95	273.29	232.97	111.74	177.72	327.46	243.57	261.87	225.01	226.70
Y	25.29	22.58	19.67	18.57	22.70	15.19	11.10	17.22	18.79	19.54	19.15
Zr	182.19	182.50	189.25	94.98	102.66	132.37	130.62	107.33	113.09	91.31	92.76

(*continued on next page*)

Table 3 (*continued*)

	18GH-01	18GH-02	18GH-03	18GH-04	18GH-05	18GH-06	18GH-07	18GH-08	18GH-09	18GH-10	18GH-11
Nb	12.66	12.62	12.14	10.01	11.12	10.20	38.91	10.34	10.76	10.01	10.16
Sn	4.66	11.88	5.26	9.83	14.74	2.77	25.14	7.27	8.09	9.08	7.34
Cs	22.12	22.63	27.24	18.75	13.91	20.07	33.53	24.20	20.84	25.17	26.33
Ba	464.63	401.30	551.47	552.32	353.38	539.54	370.08	634.86	574.47	562.13	548.56
La	43.00	42.06	40.61	31.94	35.41	32.67	78.45	32.48	41.02	33.76	29.18
Ce	83.18	81.14	76.57	61.57	72.60	66.61	175.58	61.26	78.25	65.38	58.18
Pr	8.79	8.42	8.02	6.44	7.97	7.13	16.70	6.43	8.11	6.83	6.16
Nd	30.43	29.26	26.82	21.81	28.05	24.55	57.95	21.63	27.31	24.30	22.71
Sm	5.47	4.88	4.55	4.09	5.68	4.25	8.79	3.92	4.64	4.48	4.30
Eu	1.09	1.00	0.99	0.81	0.61	0.81	1.21	0.84	0.87	0.81	0.73
Gd	4.80	4.46	3.95	3.36	4.52	3.14	4.53	3.34	3.78	3.91	3.67
Tb	0.75	0.68	0.60	0.55	0.69	0.49	0.54	0.55	0.56	0.59	0.58
Dy	4.50	3.97	3.48	3.06	4.03	2.78	2.38	2.93	3.17	3.33	3.17
Ho	0.84	0.76	0.65	0.63	0.71	0.52	0.37	0.57	0.64	0.63	0.67
Er	2.35	2.09	1.82	1.81	1.98	1.46	1.01	1.66	1.72	1.84	1.81
Tm	0.35	0.32	0.28	0.29	0.30	0.24	0.15	0.25	0.28	0.27	0.28
Yb	2.28	2.08	1.95	1.91	1.92	1.35	0.91	1.57	1.78	1.73	1.65
Lu	0.32	0.33	0.29	0.28	0.29	0.19	0.14	0.24	0.29	0.28	0.25
Hf	4.88	4.81	5.08	2.78	3.28	3.64	4.01	2.91	3.15	2.82	2.80
Ta	1.18	0.90	1.02	1.20	1.15	0.87	11.30	1.09	1.16	1.20	1.31
Tl	0.81	0.89	0.98	1.10	1.31	1.17	1.33	1.21	1.03	1.11	1.10
Pb	26.27	41.39	22.43	30.03	40.99	27.21	37.63	31.42	29.12	30.27	27.22
Th	15.41	18.39	18.07	14.69	24.78	16.71	55.59	14.39	20.75	16.62	15.83
U	2.66	3.88	4.14	3.83	8.53	3.56	17.51	4.47	9.00	5.61	4.06

REFERENCES

Ahmadi P., Dincer I., Rosen M.A., 2013. Performance assessment and optimization of a novel integrated multigeneration system for residential buildings. Energy Build 67, 568-578. https://doi.org/10.1016/j.enbuild.2013.08.046.

Bao, Z., Peng, J.B., Zhang, J., 2009. Development and distribution patterns of active faults zone in Qinghai Province. J. Eng. Geol. 17, 612–618 (in Chinese).

Boynton, W.V., 1984. Cosmochemistry of the rare earth elements: meteorite studies. In: Henderson, P.E. (Ed.), Rare Earth Element Geochemistry. Elsevier, Amsterdam. pp. 63–114.

Feng, Y.F., Zhang, X.X., Zhang, B., 2018. The geothermal formation mechanism in the Gonghe Basin: Discussion and analysis from the geological background. China Geology 3, 331-345 (in Chinese with English abstract).

Genter A., Evans K., Cuenot N., 2010. Contribution of the exploration of deep crystalline fractured reservoir of Soultz to the knowledge of enhanced geothermal systems (EGS), Compt. Rendus Geosci. 342, 502-516.

Habka M, Ajib S., 2013. Determination and evaluation of the operation characteristics for two configurations of combined heat and power systems depending on the heating plant parameters in low-temperature geothermal applications. Energy Convers Manag, 6, 996-1008. https://doi.org/10.1016/j.enconman.2013.08.046.

Hou, K.M., Shi, Y.M., Zhang, X., 1999. Activity ways and formation age of the NNW tectonics in the northern Tibet plateau. Seismolog. Geol. 21, 127-136.

Hu, Z.C., Zhang, W., Liu, Y.S., 2015. "Wave" signal smoothing and mercury removing device for laser ablation quadrupole and multiple collector ICP-MS analysis: application to lead isotope analysis. Analytical Chemistry 87, 1152-1157.

Lei, Z.H., Zhang, Y.J., Yu, Z.W., 2019. Exploratory research into the enhanced geothermal system power generation project: The Qiabuqia geothermal field, Northwest China. Renewable Energy 139, 52-70.

Liu, Y.S., Gao, S., Hu, Z.C., 2010. Continental and oceanic crust recycling-induced melt-peridotite interactions in the Trans-North China Orogen: U-Pb dating, Hf isotopes and trace elements in zircons of mantle xenoliths. Journal of Petrology 51, 537-571.

Liu, Y.S., Hu, Z.C., Gao, S., 2008. In situ analysis of major and trace elements of anhydrous minerals by LA-ICP-MS without applying an internal standard. Chemical Geology 257, 34-43.

Lu, H.J., Wang, E., Shi, X.H., 2012. Cenozoic tectonic evolution of the Elashan range and its surroundings, northern Tibetan Plateau as constrained by paleomagnetism and apatite fission track analyses. Tectonophysics 580, 150-161.

Ludwig, K.R., 2003. ISOPLOT 3.00: A Geochronological Toolkit for Microsoft Excel. Berkeley Geochronology Center, California, Berkeley. pp. 39.

Sun, S. S., McDonough, W.F., 1989. Chemical and isotopic systematics of oceanic basalts: implications for mantle composition and processes. In: Saunders, A.D., Norry, M.J. (Eds.), Magmatism in the Ocean Basins. Geological Society of London Special Publications 42. pp. 313–345.

Sun, Z.X., Li, B.X., Wang, Z.L., 2011. Exploration of the possibility of hot dry rock occurring in the Qinghai Gonghe basin. Hydrogeol. Eng. Geol. 38, 119–151 (in Chinese).

Tapponnier, P., Xu, Z.Q., Roger, F., 2001. Geology-oblique stepwise rise and growth of the Tibet plateau. Science 294, 1671–1677.

Tester J.W., Anderson B.J., Batchelor A.S., 2006. The future of geothermal energy - impact of enhanced geothermal systems (EGS) on the United States in the 21st century. MIT - Massachusetts Inst Technol. pp. 358.

Wang G., Li K., Wen D., 2013. Assessment of geothermal resources in China. Thirty-Eighth Work. Geotherm. Reserv. Eng. 10.

Wang, B., Li, B.X., Ma, X.H., 2015. The prediction of the depth and temperature of the reservoir in the evaluation of hot dry rock (HDR) for Gonghe-Guide basin. Ground Water 37, 28–31.

Xie L., Min K.B., 2016. Initiation and propagation of fracture shearing during hydraulic stimulation in enhanced geothermal system. Geothermics 59, 107-120. https://doi.org/10.1016/j.geothermics.2015.10.012.

Xie, X.L., Niu, M.L., Wu, Q., 2015. Petrological characteristics of Triassic magmatic rocks from the conjunction of Qinling, Qilian, and Kunlun Orogens and their tectonic environment. Journal of Earth Sciences and Environment 37(6), 72-81.

Xu, T.F., Yuan, Y.L., Jia, X.F., 2018. Prospects of power generation from an enhanced geothermal system by water circulation through two horizontal wells: A case study in the Gonghe Basin, Qinghai Province, China. Energy 148, 196-207.

Xue, J.Q., Gan, B., Li, B.X., 2013. Geological-geophysical characteristics of enhanced geothermal system (hot dry rock) in Gonghe-Guide basin. Geophys. Geochem. Explor 37, 35–41.

Yan, W.D., Wang, Y.X., Gao, X.Z., 2013. The distribution and aggregation mechanism of geothermal energy in Gonghe basin. Northwest Geol. 46, 223–230 (in Chinese).

Yin, A., Harrison, T.M., 2003. Geologic evolution of the Himalayan-Tibetan orogen. Annu. Rev. Earth Planet. Sci. 28, 211–280.

Zarrouk S.J., Moon H., 2014. Efficiency of geothermal power plants: a worldwide review. Geothermics 51, 142-153. https://doi.org/10.1016/j.geothermics.2013.11.001.

Zhang, C., Jiang, G.Z., Shi, Y.Z., 2018a. Terrestrial heat flow and crustal thermal structure of the Gonghe-Guide area, northeastern Qinghai-Tibetan plateau. Geothermics, 72, 182-192.

Zhang, H.F., Chen, Y.L., Xu, W.C., 2006. Granitoids around Gonghe basin in Qinghai province: petrogenesis and tectonic implications. Acta Petrologica Sin. 12, 2910–2922 (in Chinese).

Zhang, S.Q., Yan, W.D., Li, D.P., 2018b. Characteristics of geothermal geology of the Qiabuqia HDR in Gonghe Basin, Qinghai Province. Geology in China 45(6), 1087-1102(in Chinese with English abstract).

Ziagos J., Phillips B.R., Boyd L., 2013. Technology roadmap for strategic development of enhanced geothermal systems, in: Proceedings of Thirty-Eighth Workshop on Geothermal Reservoir Engineering, Stanford University, Stanford, California, February 11-13, SGP-TR-198.

Zong, K.Q., Klemd, R., Yuan, Y., 2017. The assembly of Rodinia: The correlation of early Neoproterozoic (ca. 900 Ma) high-grade metamorphism and continental arc formation in the southern Beishan Orogen, southern Central Asian Orogenic Belt (CAOB). Precambrian Research 290, 32–48.